



Fabrication of three-dimensional orthodontic force detecting brackets and preliminary clinical test for tooth movement simulation

Qianyang Xie^{a,1}, Li Peilun^{a,1}, Zhou Zhitao^b, Bai Guo^a, Sun Ke^b, Li Xinxin^b,
Tao Tiger Hu^b, Yang Heng^{b,***}, Zou Duohong^{a,**}, Yang Chi^{a,*}

^a Ninth People's Hospital, College of Stomatology, Shanghai Jiao Tong University School of Medicine, Shanghai Key Laboratory of Stomatology and Shanghai Research Institute of Stomatology, No. 639, Zhizaoju Rd., Shanghai, 200011, China

^b Shanghai Institute of Microsystem and Information Technology (SIMIT), Chinese Academy of Sciences, No. 865, Changning Rd., Shanghai, 200050, China

ARTICLE INFO

Keywords:

Force detection bracket
Pressure sensor
In vivo force measurement
Mechanical simulation model
Tooth movement

ABSTRACT

This study aimed to develop an ultraminiature pressure sensor array to measure the force exerted on teeth. Orthodontic force plays an important role in effective, rapid, and safe tooth movement. However, owing to the lack of an adequate tool to measure the orthodontic force in vivo, it remains challenging to determine the best orthodontic loading in clinical and basic research. In this study, a three-dimensional (3D) orthodontic force detection system based on piezoresistive absolute pressure sensors was designed. The 3D force sensing array was constructed using five pressure sensors on a single chip. The size of the sensor array was only 4.1×2.6 mm, which can be placed within the bracket base area. Based on the barometric calibration, conversion formulas for the output voltage and pressure of the five channels were constructed. Subsequently, a 3D linear mechanical simulation model of the voltage and stress distribution was established using 312 tests of the applied force in 13 operating modes. Finally, the output voltage was first converted to pressure and then to the resultant force. The 3D force-detection chip was then tested to verify the accuracy of force measurement on the teeth. Based on the test results, the average output force error was only 0.0025 N (0.7169%) ($p = 0.958$), and the average spatial positioning error was only 0.058 mm ($p = 0.872$) on the X-axis and 0.050 mm ($p = 0.837$) on the Y-axis. The simulation results were highly consistent with the actual force applied (intraclass correlation coefficient (ICC): 0.997–1.000; $p < 0.001$). Furthermore, through in vivo measurements and a finite element analysis, the movement trends generated when the measured orthodontic forces that acted on the teeth were simulated. The results revealed that the device can accurately measure the orthodontic force, representing the first clinical test of an orthodontic-force monitoring system. Our study provides a hardware basis for clinical research on efficient, safe, and optimal

* Corresponding author. Department of Oral Surgery, Ninth People's Hospital, Shanghai Jiao Tong University School of Medicine, 639 Zhizaoju Road, Shanghai, 200011, China.

** Corresponding author. Department of Oral Surgery, Ninth People's Hospital, Shanghai Jiao Tong University School of Medicine, 639 Zhizaoju Road, Shanghai, 200011, China.

*** Corresponding author. Shanghai Institute of Microsystem and Information Technology (SIMIT), Chinese Academy of Sciences, 865, Changning Road, Shanghai, 200050, China.

E-mail addresses: h.yang@mail.sim.ac.cn (Y. Heng), zouduohongyy@163.com (Z. Duohong), yangchi63@hotmail.com (Y. Chi).

¹ These authors have distributed equally and are co-first authors.

<https://doi.org/10.1016/j.heliyon.2023.e19852>

Received 9 February 2023; Received in revised form 26 August 2023; Accepted 4 September 2023

Available online 14 September 2023

2405-8440/© 2023 The Authors. Published by Elsevier Ltd. This is an open access article under the CC BY-NC-ND license (<http://creativecommons.org/licenses/by-nc-nd/4.0/>).

orthodontic forces, and has considerable potential for application in monitoring the biomechanics of tooth movement.

1. Introduction

The development and commercial application of wearable electronic devices in medicine and healthcare have made the monitoring of physiological parameters in daily activities increasingly timely, accurate, and convenient [1]. Forces play important roles in regulating the functional activities of molecules, cells, and tissues in living organisms. Orthodontics with fixed appliance is a therapy that guides the movement of teeth by external force to ultimately achieve aesthetic and functional improvement of teeth, which is widely needed because the number of malocclusion patients seeking help is numerous [2]. Orthodontic brackets are components of fixed orthodontic appliances which are bonded to the patient's teeth to hold the arch wires that apply a constant force on every tooth, creating a mechanical load on the soft tissue (periodontal ligament) between the root and the alveolar bone. This load causes alveolar bone remodelling, resulting in tooth movement [3–5].

Application of an optimal orthodontic force is vital for improving the efficiency and outcome of orthodontic treatment; however, determining the ideal force for clinical and basic research still remains challenging [6]. The magnitude and actuation duration of orthodontic force are important factors influencing the incidence and severity of complications, such as severe root resorption, alveolar bone cracking, and pain; which could be the result of excessive load and prolonged stress concentration [7–9]. Many attempts have been made to determine the magnitude of force exerted on teeth during orthodontic treatment, including clinical trials and animal experiments, finite element method (FEM)-based mechanical simulations, in vitro sensors-driven model testing, and sensorised bracket models [10–12]. However, accurate measurements of orthodontic force in vivo have not yet been achieved. As the orthodontic force is a 3D force/torque, which is very complex and variable, it is necessary to use high-precision sensor arrays to achieve measurement and force synthesis in all directions. It is generally believed that the force exerted on a single tooth during orthodontic treatment should not exceed its root surface area (cm^2) \times 26 gf; that is, only 35–80 gf for a single-rooted tooth [13].

Therefore, the precision sensor used must be of high calibre in terms of volume, range, accuracy, and sensitivity, and most importantly, small, and thin enough to form an array which fits in a tiny bracket. The ultrasmall pressure sensors reported by Jiao et al., in 2020 [14], which were manufactured via the microelectromechanical system (MEMS) technique, have a high precision and spatial resolution, and each sensor was only 0.4×0.4 mm in area and 0.25 mm in height. Using this tiny sensor, it was possible to form a sensorised orthodontic bracket without considerably changing much of its original shape and structure.

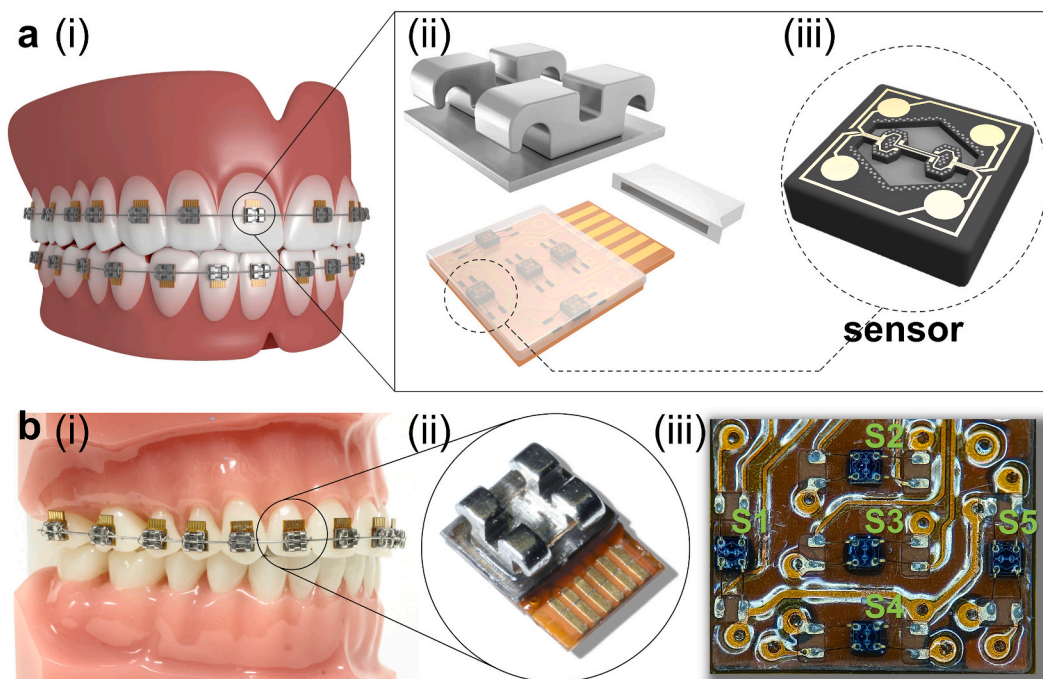


Fig. 1. Design and fabrication of force detection bracket.

a. Schematic of full dentition and stress monitoring bracket design (i), bracket and circuit board internal structure (ii), sensor form used (iii). **b.** Fabricated stress monitoring brackets. The brackets are bonded to tooth model and the orthodontic arch wire is ligated and fixed (i), an individual bracket (ii), and the photo of the sensor connected to the circuit board during the production process (iii).

The aim of this study was to develop an ultraminiature pressure sensor array to measure the force exerted on teeth. Hence, in this study, we report the fabrication of a three-dimensional orthodontic-force detection bracket and the first in vivo measurement of orthodontic force with a sensorised bracket. In a preliminary study, an FEM-based analysis of a bracket bonded to a tooth was employed to simulate the interrelationships between the orthodontic force and the resulting mechanical stress distributions within the bracket base (Supplementary Figs. 1 and 2, and Supplementary Table 1). Accordingly, the sensor array consisted of five pressure sensors arranged orthogonally in the gingival-incisal and medial-distal directions with a layout of three sensor units per row (Fig. 1a and b). Subsequently, a pilot clinical test was conducted on a volunteer to acquire data on the actual force, and a simulation of the tooth movement trend was performed using FEM. Our goal was to use a pressure sensor array to accurately measure the force exerted on the tooth by the appliance, thereby improving orthodontic force control and the efficiency and safety of orthodontic treatment.

2. Materials and methods

2.1. Fabrication of the orthodontic force detection bracket

Five sensor units were assembled in a chip area of 2.9 × 4.1 mm. The flexible printed circuit (FPC) was reinforced with polyimide (PI) to stabilise the plane on which the sensor was located. Gold wire bonding process was used to connect the sensor to the circuit, and an epoxy resin (Loctite Ccobond Ablestik 2332 Non-conductive adhesive, Henkel Lutel, Dusseldorf, Germany) was used to secure the sensor and welding wire arc. Elastosil E43 medical silicone adhesive (Wacker Chemie GmbH, Germany) was used to fill the gap between the sensors and bond the brackets (upper right central incisors, edgewise bracket with slot of 0.022 × 0.028 inch, 936-304R; Tomy Inc., Fukushima Prefecture, Japan) to the chip. The surface of the circuit except for the gold finger was covered with a 2 μm Parylene film by the meteorological growth method to prevent the circuit from being eroded by body fluids. The bracket was modified and the distance from the bottom of the slot to the base plate was shortened to make room for the sensing chip.

A pluggable wired transmission was used for digital communication and energy supply to read the data and provide power. On the gingival side of the circuit board, a double-sided 12-pin gold finger connection was designed. The connection and data acquisition devices were designed and produced.

2.2. Calibration and electrical-mechanical benchmarking

Electrical-mechanical benchmarking was performed in two steps (Fig. 2). First, calibration was performed to establish the

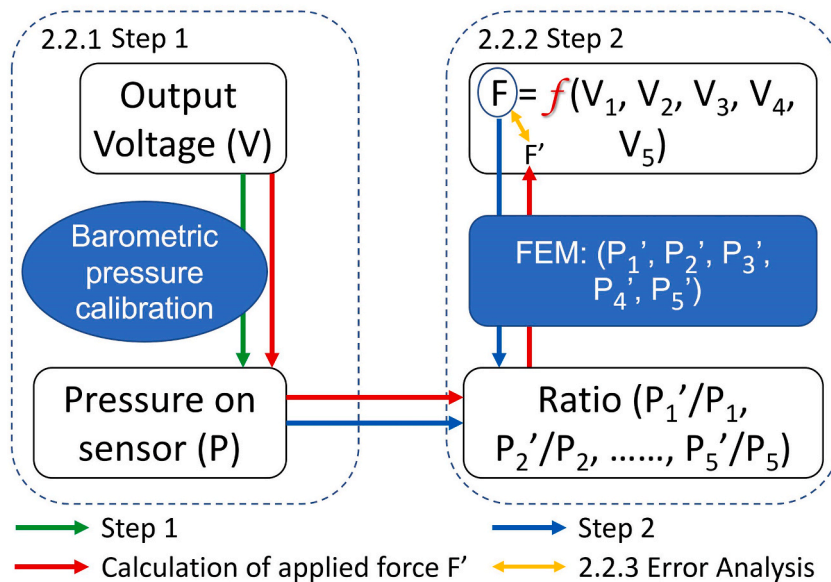


Fig. 2. Flowchart of calibration and electrical-mechanical benchmarking.

In step 1, five sensor units were calibrated with atmospheric pressure separately. Pressure values and output voltages were analysed with linear regression. In step 2, all five sensors were encapsulated within a bracket and responded simultaneously to one applied force (F) by giving output voltages (V₁, V₂, V₃, V₄, V₅). Using the linear relationship gained in step 1, the output voltages were converted into pressure values (P₁, P₂, P₃, P₄, P₅). At the same time, the applied force (F) was loaded onto the sensor chip FEM model, through simulations of stress distribution, thus obtaining pressure on sensors (P₁', P₂', P₃', P₄', P₅'). P and P' were compared to establish associations between electrical and mechanical systems. Thus, the output voltages could be converted into pressure values, which should be further multiply ratio P'/P, and then through a reversed procedure of the FEM, the exerted force could be simulated (F'). Finally, the simulated force (F') and the actual applied force (F) were compared, and the error of electrical-mechanical conversion was calculated.

conversion from voltage to pressure. Subsequently, the FEM was employed to analyse the relationship between the pressure on the sensor units and the applied force. All five sensors were encapsulated within a bracket and responded simultaneously to an applied force (F) by providing output voltages ($V_1, V_2, V_3, V_4,$ and V_5). Using the linear relationship obtained in the first step, the output voltages were converted into pressure values ($P_1, P_2, P_3, P_4,$ and P_5). The pressure on each sensor was also acquired through FEM simulation and recorded as $P_1', P_2', P_3', P_4',$ and P_5' . The electrical output of the sensors and the actual applied force were benchmarked by the ratio P'/P . Thus, the output voltages could be converted into pressure values, which were further multiplied by P'/P , and subsequently, through a reversed procedure of the FEM, the applied force (F') could be simulated.

2.2.1. Calibration of the sensors

The first step, calibration with barometric pressure was performed before the chips were assembled onto the brackets. A direct-current powered analyser (N6705C, Keysight, Beijing, China) was used as the power supply, and was set to 3.3 V. An Agilent 34401A 6 1/2 Digit Multimeter was used to read the output voltage. The wired, unpackaged chip was placed in a sealed, airtight testing box (Supplementary Fig. 3), and a GE Druck DPI 104 digital standard pressure gauge (Supplementary Fig. 3) was used to adjust the pressure in the testing box.

By loading the atmospheric pressure (60, 84, 101.03, 110.47, 129.78, and 145.76 kPa) on the chip, six output voltages were recorded from each sensor. The pressure was maintained static when the results were recorded. Linear regression of the output voltage with the pressure was performed for each sensor to establish the conversion from voltage to pressure.

2.2.2. Relationship between pressure on sensor units and applied force

After the encapsulation, the relationship between the pressure on each of the five sensors in the stress-monitoring bracket and the force exerted was determined. The bracket base was placed upward and fixed parallel to the horizontal plane on a universal test bench. A digital force meter with a range of 10 N and a resolution of 0.001 N (SH-10 N, Nscing Es Su Test, Nanjing, Jiangsu) was used to apply force to the bracket base. Thirteen different sites were selected for force exertion using 13 operating modes (OM). A static pressing force of 0–0.784 N (0–80 gf) was used for each OM, and the load was increased by 0.098 N per test, and this was repeated thrice. The five channels of output voltage data of each OM were acquired at a frequency of 800 Hz for 6.4 s in each test. A coordinate system was established with the centre of the bracket base plate as the origin, with the X-axis in the medial-distal direction and the Y-axis in the gingival-incisal direction.

In this step, an FEM with a second-order hexahedral mesh was utilised to simulate the stress contour when the force boundary was set on the force detection bracket. The simulations considered the stress distribution on the force detection bracket when an applied force was loaded onto the sensor chip model, which consisted of a bracket baseplate, medical silicone, epoxy bonding vinyl, silicone on the sensitive film surface, a sensor element, and PI-reinforced FPC boards (Supplementary Fig. 4 and Supplementary Table 2). The resulting stress and pressure values were used to establish the relationship with an electrically collected pressure using linear regression obtained from the calibration.

Finally, the output voltage was converted to pressure, and subsequently to the resultant force after correcting for the actual applied force.

2.2.3. Randomized testing of electrical-mechanical conversion

Afterwards, a second test was conducted to verify the accuracy of the electrical–mechanical benchmarking. The random forces were applied twice at each action point. The random forces and output voltages were recorded separately. The simulated force (F') and actual applied force (F) were compared, and the error of the electrical-mechanical conversion was calculated.

Using the collected voltage data and the conversion relationship established above, the synthesized force acting on the chip and the coordinates of the action point were calculated. The calculated force value and coordinates were compared with the actual force magnitude and position of the action point, and the error of the stress chip was analysed.

2.3. Clinical application and numeric simulation of tooth movement trend

A high resolution cone beam CT (CBCT) data with voxel spacing of $0.2 \times 0.2 \times 0.2 \text{ mm}^3$ of volunteer's premaxilla region was obtained using Planmeca ProMax® 3D Max (Planmeca Oy, Helsinki, Finland) and saved in the DICOM format. Subsequently, 3D reconstruction was performed to obtain 3D models of teeth, periodontal membrane, cancellous bone, and cortical bone to establish a mechanical model of dental-periodontal tissue by FEM. A 3D orthodontic force detection bracket was used to measure the actual force on the volunteer's right upper central incisor; regular canal-shaped brackets were fixed on the buccal side of the bilateral maxillary first molars, and rubber elastic chains were used to apply a retraction force on the central incisor. Two sets of output voltage data were collected, including the retraction of the upper anteriors by a short and a long hook, and the elastic chain was used to exert a retracting force of 0.588 N (60 gf). The brackets and elastics were removed immediately after data collection.

A hexahedral finite element analysis simulation model was employed to examine the mechanism of tooth movement. The force data generated by the sensor array was applied to the tooth model as the line pressure at the interface between the chip and base plate, serving as the initial condition [15,16]. In this model, with 75520 elements, 29821 nodes, and periodontal ligament thickness ranging from 0.2 to 0.4 mm, the two ends of the alveolar bone were fixed.

2.4. Declaration

The study was conducted in accordance with the Declaration of Helsinki and approved by the ethics committee (Institutional Review Board of Shanghai Ninth People's Hospital, SH9H-2022-T395-1). All participants were fully informed and provided written informed consent before participating in the study.

3. Results

The sensor array is only 4.1×2.6 mm except for the gold finger region, which is suitable for the bracket base. Subsequently, the conversion relationship between the voltage and orthodontic force was established. The actual exerted force was highly consistent with the simulation results; the output force error was only 0.7169%, and the average error of spatial positioning was only 0.054 mm. The movement trends generated when the measured orthodontic forces acting on the tooth were simulated through in vivo measurements and FEM.

3.1. Device morphological structure

An optical micrograph of the sensor chip showed the circuit structure of the chip; the sensors were numbered S1–S5, as shown (Fig. 1b and Supplementary Fig. 5). The area of the sensor array was 4.1×2.6 mm, and the thickness was less than 0.5 mm. With a modified bracket, the total height of the orthodontic force-detecting bracket was almost the same as that of the normal bracket (Supplementary Fig. 5).

3.2. Characterizations and calibration of sensor array

After the ultra-small pressure sensor (Fig. 3a) was connected to the circuit board, an instantaneous change in the output voltage could be observed by gentle pressing and pulling (Fig. 3c). Through barometric pressure calibration and linear regression, the output voltage of each sensor unit was converted into pressure values (Fig. 3d). The detailed numbers of calibrations are listed in Table 1.

The encapsulated chip and bracket were further analysed using a test bench and force meter (Fig. 4a). The force application site (OMs) and its coordinates are shown in Fig. 4b. The output voltage of each sensor exhibited a good linear relationship with the applied force at 13 OMs. For example, OM3 (Fig. 4c i) and OM7 (Fig. 4c ii) were performed at symmetric locations, and the patterns of the

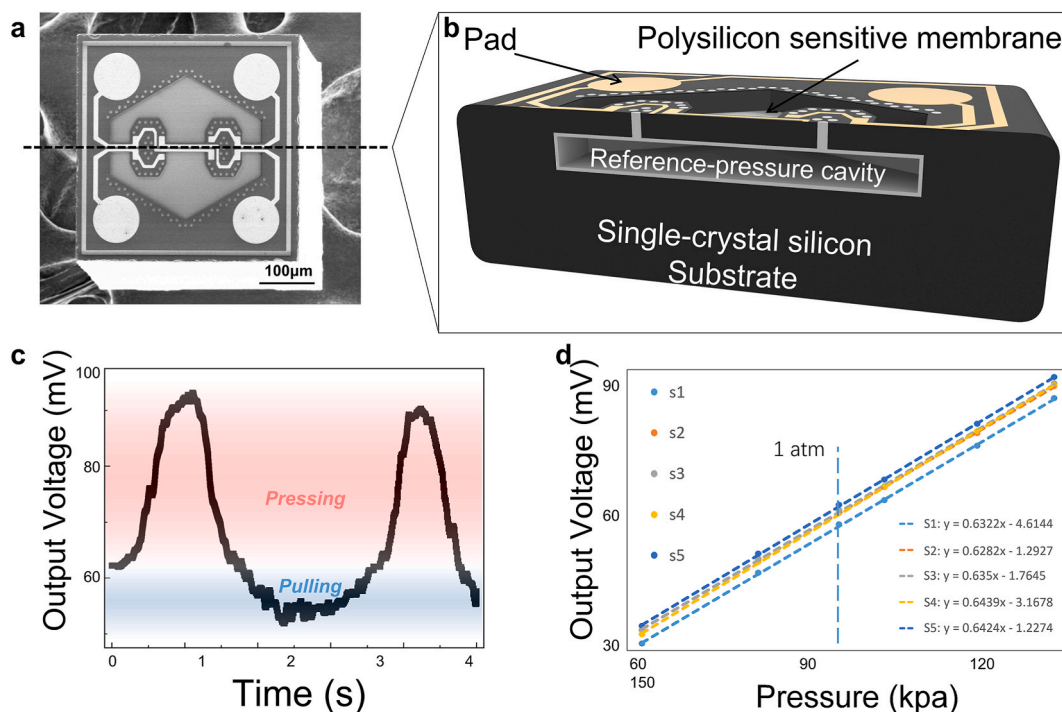


Fig. 3. Performance characterization of a single sensor.

a. Scanning electron microscope photograph of a sensor; **b.** A cross-sectional diagram of the sensor, showing the structure of reference-pressure cavity beneath the sensitive membrane; **c.** Instantaneous change in sensor output voltage with tension/pressure applied; **d.** The output voltage of sensors and linear regression with pressure.

Table 1
Barometric calibration of sensors before encapsulation.

Pressure (Kpa)	Output Voltages (mV)				
	S1	S2	S3	S4	S5
60	33.1	36.15	36.1	35.19	37.07
84.2	48.88	51.85	51.99	51.3	53.1
101.03	59.62	62.6	62.8	62.13	64
110.47	65	67.9	68.1	67.96	69.6
129.78	77.1	79.9	80.3	80.3	82
145.76	87.7	90.4	90.97	90.6	92.4

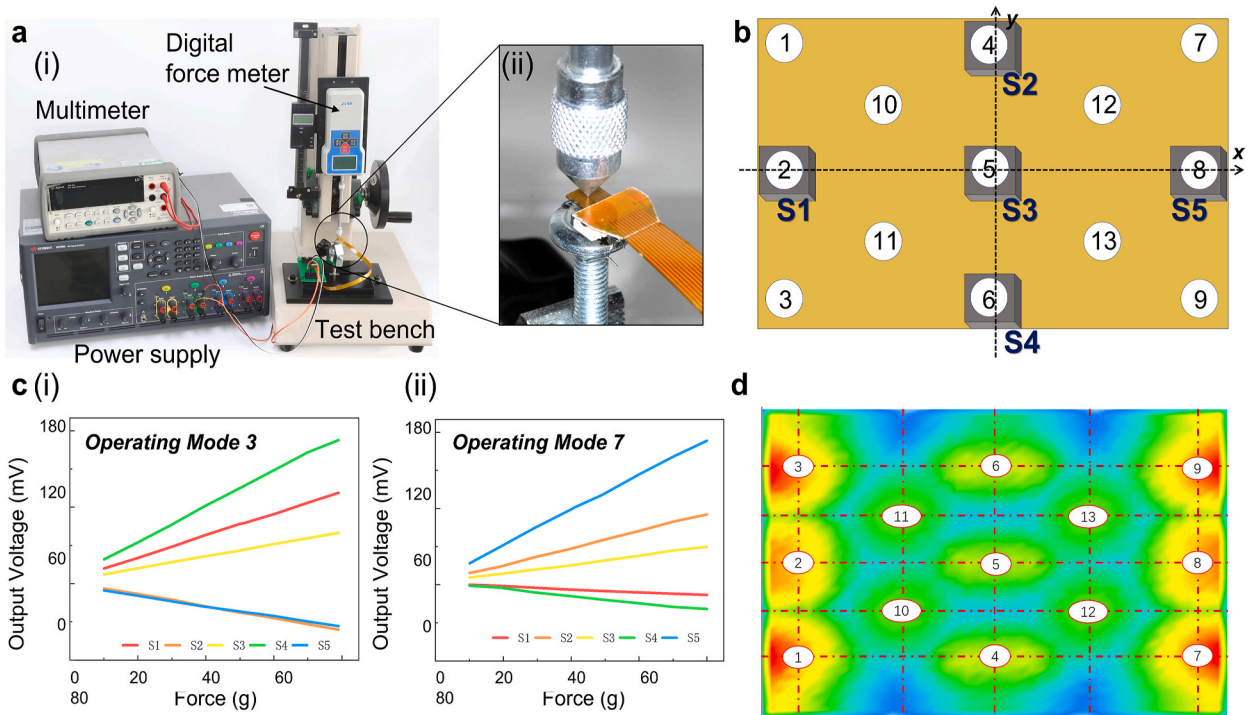


Fig. 4. Calibration of orthodontic force monitoring chip. **a.** Test environment: power supply, multimeter, test bench, push-pull force meter (i), and force applying to the bracket base plate (ii). **b.** The positions of the 13 action sites (13 operating modes, OM) and their relationship to the sensor position. **c.** Distribution characteristics of 5 channel data under different OMs, taking OM3 and OM7 as examples, (i) the output voltages of S1 and S4 increase under OM3, and the output voltages of S2 and S5 decrease, while (ii) the output voltages of S2 and S5 increase under OM7, and the output voltages of S1 and S4 decrease. **d.** Deflection effect of the chip caused by different OMs.

output voltage were opposite. Using FEM, a linear relationship between the simulated and measured pressures was observed, and conversion from the electrical signal to the resultant force was established. The positional simulation also showed a high consistency with the actual action points (Supplementary Fig. 6).

3.3. Randomized testing of electrical-mechanical conversion

Compared with the magnitude of the actual exerted force, the synthesized resultant force showed a high consistency, with an average error of 0.0025 N (0–0.009 N), an average error rate of only 0.72%, and an intraclass correlation coefficient (ICC) of 1.000 ($p < 0.001$) (Table 2). The paired *t*-test analysis showed no significant difference between the two groups ($p = 0.958$).

The actual action site applied on the sensor chip was highly consistent with the simulated action site of the resultant force ($p < 0.001$), with an ICC of 0.999 (0.998–1.000) and 0.998 (0.997–0.999) on the X-axis and Y-axis, respectively. The paired *t*-test showed no significant differences between the two sets of data, with average errors of 0.050 mm ($p = 0.872$) and 0.058 mm ($p = 0.837$) on the X-axis and Y-axis, respectively (Table 2).

Table 2
Comparison of the exerted force and the simulation synthesis force.

No.	Operating mode coordinates (mm)		Force 1 Exerted (N)	Force 1 synthesized (N)	Coordinates 1 synthesized (mm)		Force 2 Exerted (N)	Force 2 synthesized (N)	Coordinates 1 synthesized (mm)	
	X axis	Y axis			X axis	Y axis			X axis	Y axis
1	-2.04	1.65	0.098	0.099	-2.19	1.57	0.598	0.604	-1.93	1.67
2	-2.04	0	0.608	0.607	-1.93	0	0.813	0.813	-2.07	0
3	-2.04	-1.65	0.5	0.5	-2.05	-1.7	0.549	0.548	-2.15	-1.58
4	0	1.65	0.186	0.186	0.03	1.78	0.421	0.426	0.03	1.77
5	0	0	0.186	0.186	0.03	0	0.598	0.597	0.03	0
6	0	-1.65	0.196	0.196	0.03	-1.68	0.304	0.304	0.03	-1.77
7	2.04	1.65	0.402	0.397	1.91	1.73	0.48	0.485	1.99	1.73
8	2.04	0	0.186	0.188	2.07	0	0.392	0.388	2.03	0
9	2.04	-1.65	0.098	0.099	1.95	-1.7	0.196	0.194	2.13	-1.58
10	-1.02	0.95	0.481	0.485	-1.06	0.97	0.687	0.678	-1.09	0.87
11	-1.02	-0.95	0.294	0.291	-1.03	-0.87	0.491	0.495	-1.06	-0.94
12	1.02	0.95	0.196	0.194	1.04	0.86	0.598	0.604	1.08	0.89
13	1.02	-0.95	0.157	0.158	0.98	-1.01	0.505	0.499	1.14	-0.94

*Numbers were retained to three decimal places.

3.4. Simulation of tooth movement trends

This study included a volunteer for assessing simulation of tooth movement. Through FEM, the tendency of tooth movement was simulated. Initially, CT data was reconstructed from 2D images into 3D models (Fig. 5a i-ii). These reconstructed models was then imported as STLs into Hypermesh (Altair Engineering, Inc.) (Fig. 5a iii). Subsequently, a complex and delicate sensorized bracket model was conceived and affixed to the tooth, enabling detailed observations (Fig. 5a iv). Mechanical parameters of the materials in

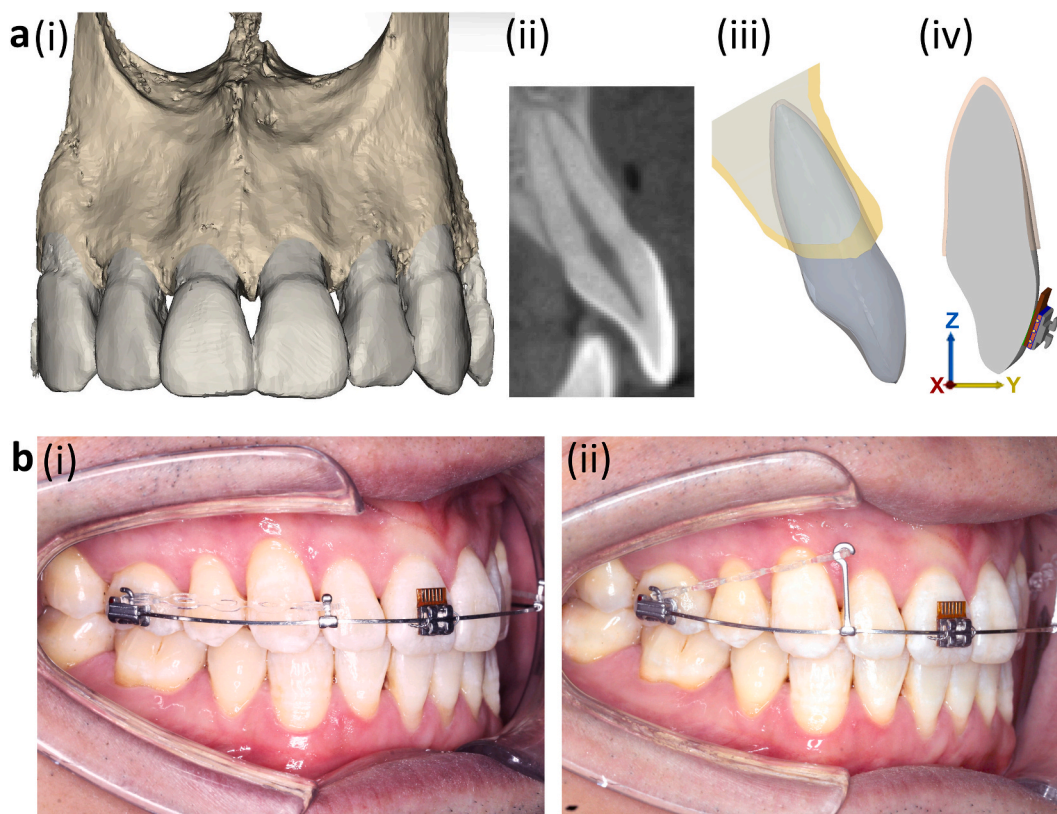


Fig. 5. Clinical test and data acquisition. **a.** Images of teeth and alveolar bone 3D reconstruction (i) were obtained by high-resolution cone beam CT scan (ii), and a FEM model of dental-periodontal membrane-alveolar bone (iii), with sensor chip array (iv) was established on this basis. **b.** The different retraction methods utilised. In the first test the elastic chain was pulled with a short hook (i), and in the other test it was pulled with a long hook (ii), and the traction force was 0.588 N.

Table 3
Mechanical property parameters of FEM.

Material	Young's modulus (MPa)	Poisson's ratio
Stainless-steel	210000	0.3
Medical silicone adhesive	800	0.4
Epoxy resin	1000	0.3
Silicone on the sensitive film surface	100	0.4
Sensitive diaphragm	300	0.2
PI circuit board	20000	0.3
Composite adhesive	8000	0.2
Enamel	84100	0.3
Dentin	18600	0.31
Periodontal ligament	8.9	0.45
Cancellous bone	1570	0.3
Cortical bone	13700	0.3

FEM were listed in Table 3. The results did not reflect the actual amount of tooth displacement, and the numerical results were 100 times magnified to illustrate the movement trends.

When a short hook was used (Fig. 5b i), the output voltage of S4 was the maximum, and all five channels were subjected to positive pressure (Fig. 6a i, ii). The maximum displacement of 11.871 μm lingually on the incisal edge, while the root apex tended to move labially, led to rotation of the tooth, with the centre of rotation in the middle of the root (Fig. 6a iii). However, when the wire was pulled with a long hook (Fig. 5b ii), the output voltage of S2 was substantially increased by positive pressure, while S4 exhibited negative pressure (Fig. 6b i, ii). The maximum displacement was only 9.347 μm lingually on the incisal edge, and the centre of rotation of the tooth was moved towards the apex with an overall rotation tendency considerably less than that with a short hook (Fig. 6b iii).

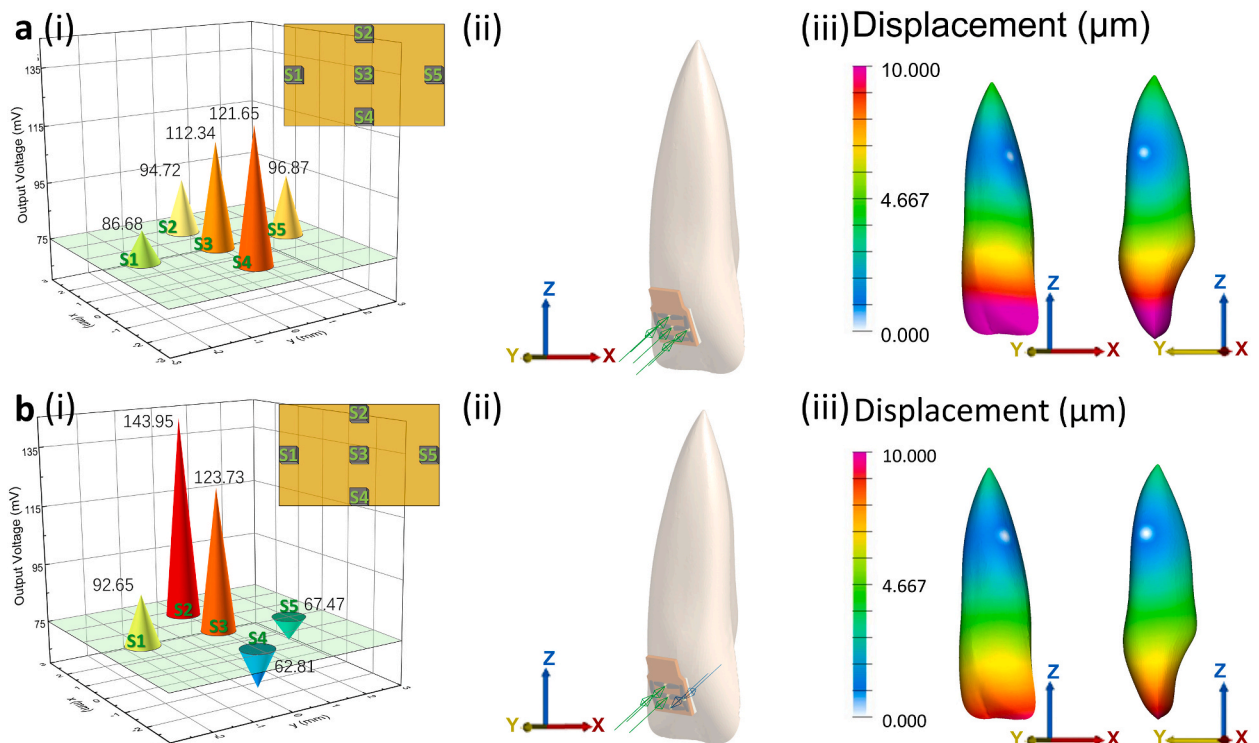


Fig. 6. Tooth movement simulation.

a. The output voltage of the sensors when the elastic chain was pulled with a short hook (i). These voltage values were then converted to stress on sensor units, and were applied to the FEM model (ii). Then, the movement trend of the tooth was simulated (iii). **b.** The output voltage of the sensors when the elastic chain was pulled with a long hook (i), and corresponding stress (ii) which was used to simulate tooth movement trend (iii).

4. Discussion

This study reports the first clinical test of a 3D orthodontic force detection bracket. We designed and fabricated stress detection chips (Fig. 1) with tiny multi-unit pressure sensors combined with brackets for the real-time monitoring of orthodontic forces. The layout of the sensor array was adapted to the bracket structure and encapsulated by a biocompatible adhesive material. The collected electrical data was converted by a linear dynamic system to a resultant force, which was further correlated with the tooth-periodontal structure through 3D imaging and FEM to simulate the trend of tooth movement. The purpose of this study was to use an ultraminiature pressure sensor array to accurately measure the force exerted on the teeth to achieve better control of the orthodontic force.

A CBCT based FEM simulation of the resultant force is beneficial in many ways. First, the rigid bonding of brackets to the teeth and the precondition of fixed orthodontic treatment meant that the conduction of orthodontic force from the bracket to the periodontal ligament should be the subject of the orthodontic mechanism; especially when studying the effect of momentum, the bracket and the tooth should be considered as a whole. Second, in vitro studies are completely different from in vivo studies. The structure around the root is complex and needs to be reconstructed using high-resolution imaging techniques to analyse the resistance around the root. For example, an orthodontic force applied at a point far from the centre of bone resistance would cause more rotation than that of an action point closer to the centre of bone resistance. Finally, in the design of the sensor array, we noticed that a resultant force could be calculated from multiple pressure values, and at the same time, each pressure value could output as stress and interact with tooth model separately to generate movement trends. These results can then be combined to predict tooth movement. Thus, the in vitro numerical simulation was minimised which induced fewer errors.

Orthodontically induced dehiscence and fenestration, as well as root resorption happen more frequently in the anterior region, as retraction of protrusive anterior teeth is a common scenario which requires the extraction of first premolars and a long duration of active orthodontic forces [17–21]. Therefore, an orthodontic force detection bracket and FEM were applied to measure the retraction force on the upper incisor and simulate the moving tendency. As the goal of this project was to achieve a timely detection of excessive load and predict tooth movement trends to eliminate complications and avoid unwanted tooth movement, the clinical testing of our device simulating the most common orthodontic scenario was valued.

The conception of using a pressure sensor to measure the orthodontic force was a great idea; however, the appropriate sensor was not readily available. It is generally believed that the force exerted on a single tooth during orthodontic treatment should not exceed its root surface area (cm^2) \times 26 gf; that is, only 35–80 gf per tooth in the anterior region [13,22–24]. Recently, our collaborator developed the smallest absolute pressure sensor with a sensitive pressure sensing, high accuracy, high signal linearity, and a small drift [14], suggesting that it is an ideal sensor for monitoring orthodontic force. A tiny absolute-pressure sensor was manufactured using a complex single-side procedure, and a reference cavity was formed beneath the sensitive diaphragm. Instead of measuring the strain caused by the applied pressure directly in a strain gauge, the pressure sensor used the elastic deformation of the thin diaphragm to measure the difference between the applied and vacuum pressures in the reference cavity. The sensitivity of a pressure sensor can be higher than that of a strain gauge when a thin diaphragm is employed. The beam-island-reinforced structure helped reduce deflection and improved the linearity in our design (Fig. 3b). In addition, the accuracy of the FEM simulations was high, owing to the use of a second-order hexahedral mesh. As a result, compared with the previously reported sensorised bracket model, which had an average error of 0.03 N [11], our force-detecting bracket yielded results with an average error of only 0.0025 N.

The space available for the stress monitoring chip was limited. The base plate of the bracket was approximately 4×3 mm in area, and the distance from the bottom of the slot to the tooth surface was not changed which necessitated the use of a tiny pressure sensor (0.4×0.4 mm in area and 0.25 mm in height) for our research.

Other advantages of our orthodontic-force monitoring system included good biocompatibility, a fairly simple structure, and data transmission, which facilitated quick approval of this study for clinical testing. Owing to its excellent biocompatible property, Parylene [25] is used as a wrapping material during implantation of transcatheter pacemakers in humans. The chip was completely covered by Parylene, which not only played a role in waterproofing and anti-corrosion, but also avoided any potential effects of circuit work on the human body. In addition, a biocompatible medical silicone adhesive was used as the encapsulation material in the heart sensor [26], which was a bonding material with good mechanical properties. The Young's modulus after curing was approximately 800 MPa, which can not only conduct an orthodontic force effectively, but also has competent mechanical strength that can protect the sensor from damage. The oral environment is complex, and teeth perform the functions of cutting, biting, and chewing food, even during orthodontic treatment. It is difficult to avoid large external impacts, which result in damage to precision devices. Through a pluggable wired transmission to read data and provide power, the circuit structure of the device was simplified as much as possible under the premise of meeting the mechanical requirements, which not only reduced the possibility of errors but also avoided potential failures.

Although our sensorised bracket prototype had certain limitations, its prospects are promising. The tooth movement trajectories after an orthodontic revisit and an orthodontic force could not be analysed using a simple linear fitting. After the final production of the orthodontic-force monitoring bracket, a continuous change in the curve of the orthodontic force with time was obtained. Simultaneously, a dataset of tooth movement trajectories was obtained by CBCT and intraoral optical scanning. The timelines during which the two datasets were collected coincided; therefore, a polynomial fitting can be used to describe the association between them. This relationship is also affected by the metabolic processes including, bone remodelling and calcium and phosphorus levels in the blood. Therefore, to achieve a state of orthodontic force and tooth movement similar to that in human body, these factors need to be incorporated in the above model through artificial intelligence analysis. Thus, to detect overwhelming stress or unwanted movement trends, clinicians can adjust how they apply force to the teeth. Personalised orthodontic systems can be developed based on this concept. To complete this force-detecting system, sensors that respond to shear force should be added to this chip, which has already been attempted. In addition, converting analogue signals into digital signals and using wireless technology to power and read data

would make clinical applications more convenient [27]. Additionally, clear aligners are gaining more popularity. Thermoplastic materials with desirable physical properties have been studied for the provision of a low continuous orthodontic force [28,29], and piezoresistive stress sensors have been applied to assess the force exerted by aligners on the teeth [30]. With our ultraminiature absolute pressure sensor and flexible printed circuit, there is a chance to develop a force monitoring system for clear aligners in the near future.

5. Conclusion

This study aimed to detect the orthodontic force applied to each tooth by setting sensors at the bottom of orthodontic brackets, which enabled clinicians to intuitively assess the 3D force direction of each tooth. Using the pressure sensor array chip developed by our research group, this study demonstrated that an orthodontic-force monitoring system could accurately measure the orthodontic force in vivo, providing a hardware foundation and basic feasibility for clinical and basic research on the orthodontic force enabling efficient, safe, and comfortable orthodontic treatment.

Author contribution statement

Qianyang Xie; Li Peilun: Conceived and designed the experiments; Performed the experiments; Analysed and interpreted the data; Contributed reagents, materials, analysis tools or data; Wrote the paper.

Zhou Zhitao; Bai Guo; Sun Ke; Li Xinxin; Tao Tiger Hu: Analysed and interpreted the data; Contributed reagents, materials, analysis tools or data.

Yang Heng; Zou Duohong; Yang Chi: Conceived and designed the experiments; Contributed reagents, materials, analysis tools or data.

Data availability statement

Data will be made available on request.

Declaration of competing interest

The authors declare that they have no known competing financial interests or personal relationships that could have appeared to influence the work reported in this paper.

Acknowledgements

The IRB approval number of this study is SH9H-2022-T395-1. This study was supported by the National Natural Science Foundation of China (81870785, 82071134, 82271038), Science and Technology Commission of Shanghai Municipality [23QC1401000], CAE Fund [2023-XY-39], and the Special project for clinical research of Shanghai Municipal Health Commission (grant number: 20204Y0459).

Appendix A. Supplementary data

Supplementary data to this article can be found online at <https://doi.org/10.1016/j.heliyon.2023.e19852>.

References

- [1] Y. Guo, X. Liu, S. Peng, X. Jiang, K. Xu, C. Chen, Z. Wang, C. Dai, W. Chen, A review of wearable and unobtrusive sensing technologies for chronic disease management, *Comput. Biol. Med.* 129 (2021), 104163, <https://doi.org/10.1016/j.combiomed.2020.104163>.
- [2] G. Lombardo, F. Vena, P. Negri, S. Pagano, C. Barilotti, L. Paglia, S. Colombo, M. Orso, S. Cianetti, Worldwide prevalence of malocclusion in the different stages of dentition: a systematic review and meta-analysis, *Eur. J. Paediatr. Dent.* 21 (2) (2020) 115–122, <https://doi.org/10.23804/ejpd.2020.21.02.05>.
- [3] L.A. Jacox, N. Tang, Y. Li, C. Bocklage, C. Graves, S. Coats, M. Miao, T. Glesener, J. Kwon, N. Giduz, F.C. Lin, J. Martinez, C.C. Ko, Orthodontic loading activates cell-specific autophagy in a force-dependent manner, *Am. J. Orthod. Dentofacial Orthop.* 161 (3) (2022) 423–436.e1, <https://doi.org/10.1016/j.ajodo.2020.09.034>.
- [4] J. Lin, J. Huang, Z. Zhang, X. Yu, X. Cai, C. Liu, Periodontal ligament cells under mechanical force regulate local immune homeostasis by modulating Th17/Treg cell differentiation, *Clin. Oral Invest.* 26 (4) (2022) 3747–3764, <https://doi.org/10.1007/s00784-021-04346-0>.
- [5] A. Spitz, D. Adesse, M. Gonzalez, R. Pellegrino, H. Hakonarson, G.A. Marañón-Vásquez, A.M. Bolognese, F. Teles, Effect of micro-osteoperforations on the gene expression profile of the periodontal ligament of orthodontically moved human teeth, *Clin. Oral Invest.* 26 (2) (2022) 1985–1996, <https://doi.org/10.1007/s00784-021-04178-y>.
- [6] C.I. Theodorou, A.M. Kuijpers-Jagtman, E.M. Bronkhorst, F.A.D.T.G. Wagener, Optimal force magnitude for bodily orthodontic tooth movement with fixed appliances: a systematic review, *Am. J. Orthod. Dentofacial Orthop.* 156 (5) (2019) 582–592, <https://doi.org/10.1016/j.ajodo.2019.05.011>.
- [7] Y. Li, S. Deng, L. Mei, Z. Li, X. Zhang, C. Yang, Y. Li, Prevalence and severity of apical root resorption during orthodontic treatment with clear aligners and fixed appliances: a cone beam computed tomography study, *Prog. Orthod.* 21 (1) (2020) 1.
- [8] Y. Deng, Y. Sun, T. Xu, Evaluation of root resorption after comprehensive orthodontic treatment using cone beam computed tomography (CBCT): a meta-analysis, *BMC Oral Health* 18 (1) (2018) 116, <https://doi.org/10.1186/s12903-018-0579-2>.

- [9] Y. Sheng, H.M. Guo, Y.X. Bai, S. Li, Dehiscence and fenestration in anterior teeth : Comparison before and after orthodontic treatment, *J. Orofac. Orthop.* 81 (1) (2020) 1–9, <https://doi.org/10.1007/s00056-019-00196-4>. English.
- [10] J. Zhong, J. Chen, R. Weinkamer, M.A. Darendeliler, M.V. Swain, A. Sue, K. Zheng, Q. Li, In vivo effects of different orthodontic loading on root resorption and correlation with mechanobiological stimulus in periodontal ligament, *J. R. Soc. Interface* 16 (154) (2019), 20190108, <https://doi.org/10.1098/rsif.2019.0108>.
- [11] B.G. Lapatki, J. Bartholomeyczik, P. Ruther, I.E. Jonas, O. Paul, Smart bracket for multi-dimensional force and moment measurement, *J. Dent. Res.* 86 (1) (2007) 73–78, <https://doi.org/10.1177/154405910708600112>.
- [12] S.D. Currell, A. Liaw, P.D. Blackmore Grant, A. Esterman, A. Nimmo, Orthodontic mechanotherapies and their influence on external root resorption: a systematic review, *Am. J. Orthod. Dentofacial Orthop.* 155 (3) (2019) 313–329, <https://doi.org/10.1016/j.ajodo.2018.10.015>.
- [13] M. Murayama, Y. Namura, T. Tamura, et al., Relationship between friction force and orthodontic force at the leveling stage using a coated wire[J], *J. Appl. Oral Sci.* 21 (2013) 554–559.
- [14] D. Jiao, Z. Ni, J. Wang, X. Li, Ultra-small pressure sensors fabricated using a scar-free microhole inter-etch and sealing (MIS) process, *J. Micromech. Microeng.* 30 (6) (2020), 065012.
- [15] M.G. Roscoe, P.M. Cattaneo, M. Dalstra, O.M. Ugarte, J.B.C. Meira, Orthodontically induced root resorption: a critical analysis of finite element studies' input and output, *Am. J. Orthod. Dentofacial Orthop.* 159 (6) (2021) 779–789, <https://doi.org/10.1016/j.ajodo.2020.02.023>.
- [16] Z. Li, M. Yu, S. Jin, Y. Wang, R. Luo, B. Huo, D. Liu, D. He, Y. Zhou, Y. Liu, Stress distribution and collagen remodeling of periodontal ligament during orthodontic tooth movement, *Front. Pharmacol.* 10 (2019 Oct 24) 1263.
- [17] L. Sun, L. Yuan, B. Wang, L. Zhang, G. Shen, B. Fang, Changes of alveolar bone dehiscence and fenestration after augmented corticotomy-assisted orthodontic treatment: a CBCT evaluation, *Prog. Orthod.* 20 (1) (2019 Feb 18) 7.
- [18] Y. Sheng, H.M. Guo, Y.X. Bai, S. Li, Dehiscence and fenestration in anterior teeth: Comparison before and after orthodontic treatment, *J. Orofac. Orthop.* 81 (1) (2020) 1–9, <https://doi.org/10.1007/s00056-019-00196-4>. English.
- [19] A. Yagci, I. Veli, T. Uysal, F.I. Ucar, T. Ozer, S. Enhos, Dehiscence and fenestration in skeletal Class I, II, and III malocclusions assessed with cone-beam computed tomography, *Angle Orthod.* 82 (1) (2012) 67–74.
- [20] X. Zhang, H. Zhou, X. Liao, Y. Liu, The influence of bracket torque on external apical root resorption in bimaxillary protrusion patients: a retrospective study, *BMC Oral Health* 22 (1) (2022) 7.
- [21] R.A. Al-Qawasmī, J.K. Hartsfield Jr., E.T. Everett, L. Flury, L. Liu, T.M. Foroud, et al., Genetic predisposition to external apical root resorption in orthodontic patients: linkage of chromosome-18 marker, *J. Dent. Res.* 82 (5) (2003) 356–360.
- [22] A.M. Schwarz, Tissue changes incident to orthodontic treatment, *Fortschritte der Orthodontik in Theorie und Praxis* 2 (1932) 154–176.
- [23] Y. Gu, Q. Zhu, Y. Tang, Y. Zhang, X. Feng, Measurement of root surface area of permanent teeth in a Chinese population, *Arch. Oral Biol.* 81 (2017) 26–30, <https://doi.org/10.1016/j.archoralbio.2017.04.015>.
- [24] P. Ye, Y. Fang, L. Zhang, H. Chen, J. Guan, X. Lin, L. Wu, X. Shao, Full denture periodontal ligament anatomical modeling and measurement of a male Chinese human, *J. Media Res.* 45 (5) (2016) 71–75.
- [25] M.F. El-Chami, J. Mayotte, M. Bonner, R. Holbrook, K. Stromberg, M.R. Sohail, Reduced bacterial adhesion with parylene coating: potential implications for Micra transcatheter pacemakers, *J. Cardiovasc. Electrophysiol.* 31 (3) (2020) 712–717, <https://doi.org/10.1111/jce.14362>.
- [26] W.T. Abraham, P.B. Adamson, R.C. Bourge, M.F. Aaron, M.R. Costanzo, L.W. Stevenson, W. Strickland, S. Neelagaru, N. Raval, S. Krueger, S. Weiner, D. Shavelle, B. Jeffries, J.S. Yadav, CHAMPION Trial Study Group, Wireless pulmonary artery haemodynamic monitoring in chronic heart failure: a randomised controlled trial, *Lancet* 377 (9766) (2011) 658–666, [https://doi.org/10.1016/S0140-6736\(11\)60101-3](https://doi.org/10.1016/S0140-6736(11)60101-3).
- [27] J. Hafner, B.G. Lapatki, O. Paul, First telemetric smart orthodontic bracket for therapeutic applications[C], *IEEE Sensors Conference* 8 (1) (2018) 1–4. New Delhi.
- [28] S. Inoue, S. Yamaguchi, H. Uyama, T. Yamashiro, S. Imazato, Orthodontic aligner incorporating eucommialmoides exerts low continuous force: in vitro study, *Materials* 13 (18) (2020 Sep 14) 4085, <https://doi.org/10.3390/ma13184085>.
- [29] S. Inoue, S. Yamaguchi, H. Uyama, T. Yamashiro, S. Imazato, Influence of constant strain on the elasticity of thermoplastic orthodontic materials, *Dent. Mater. J.* 39 (3) (2020 Jun 5) 415–421, <https://doi.org/10.4012/dmj.2019-104>.
- [30] S. Yun, An ultra-thin piezoresistive stress sensor for measurement of tooth orthodontic force in invisible aligners[J], *IEEE Sensor. J.* 12 (5) (2012) 1090–1097.